SPALLATION NEUTRON SOURCE RING – STATUS, CHALLENGES, ISSUES, AND PERSPECTIVES*

Jie Wei†
for the Spallation Neutron Source Collaboration, USA

Abstract

The Spallation Neutron Source (SNS) ring is designed to accumulate beam pulses of 1.5×10^{14} protons of 1 GeV kinetic energy at a repetition rate of 60 Hz [1]. At such beam intensity and power, key design challenges include control of beam loss and radio-activation, construction of high-quality large-aperture magnets and power supplies, design of robust injection and extraction systems, minimization of beam-coupling impedances, and mitigation of electron-cloud effects. This paper discusses the status of the ring systems with emphasis on technical challenges and issues, and presents future perspectives towards a next-generation high-intensity facility.

INTRODUCTION

The SNS project is presently in the 5th year of a 7-year construction cycle [2]. The SNS ring, designed and constructed mainly by the Brookhaven National Laboratory, will accumulate pulses of 1.5×10^{14} protons of 1 GeV kinetic energy at a repetition rate of 60 Hz (Table 1) [1].

The primary concern is beam-loss induced radioactivation that can limit the ring's availability and maintainability. With a dedicated beam collimation in the ring at an efficiency above 90%, the tolerable fractional beam loss is about 10^{-3} [3].

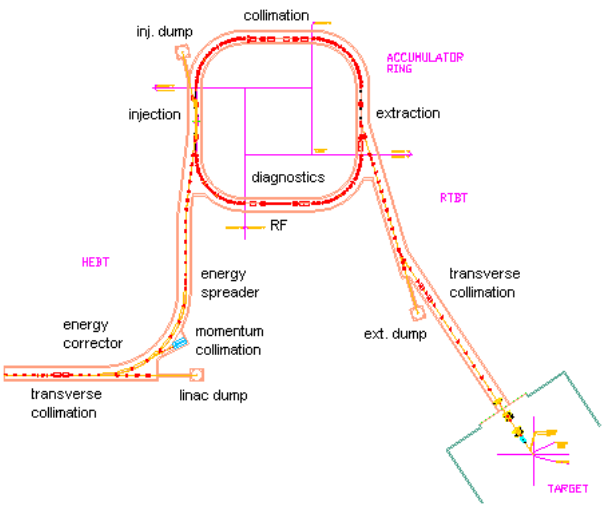

Figure 1: Layout of the SNS accumulator ring, the high-energy beam transport (HEBT), and the ring-to-target transport (RTBT).

Table 1: Major parameters of the SNS accumulator ring and its transport lines (HEBT and RTBT).

Quantity	Value
Circumference	248.0 m
HEBT, RTBT length	169, 151 m
Beam energy	1 GeV
Magnetic rigidity, $B\rho$	5.657 Tm
Average beam power	1.5 MW
Repetition rate	60 Hz
Number of protons per pulse	1.6×10^{14}
Revolution frequency	1.058 MHz
Peak RF voltage ($h = 1, 2$)	(40, 20) kV
No. of RF station (ring, HEBT, RTBT)	4, 2, 0
Unnorm. emittance ($\epsilon_x + \epsilon_y$, 99%)	240 $\pi\mu$m
Betatron acceptance	480 $\pi\mu$m
RF momentum acceptance	$\pm$ 1 %
Transverse tunes (ν_x, ν_y)	6.23, 6.20
Transition energy, γ_T	5.23
Natural chromaticities (ξ_x, ξ_y)	-7.9, -6.9
No. of super-periods	4
No. of dipole (ring, HEBT, RTBT)	39, 9, 1
Ring dipole field	0.7406 T
Ring dipole gap height	170 mm
No. of quad (ring, HEBT, RTBT)	53, 40, 32
Ring quad inner diameter	210-300 mm
No. of sextupole (ring, HEBT, RTBT)	20, 0, 0
Sextupole inner diameter	210-260 mm
No. of corrector (ring, HEBT, RTBT)	61, 18, 17
No. of kicker (injection, extraction)	8, 14
No. of scraper (ring, HEBT, RTBT)	4, 5, 0
No. of absorber (ring, HEBT, RTBT)	3, 3, 2
No. of vacuum pumps (ring, HEBT, RTBT)	50, 18, 12
No. of power supply (ring, HEBT, RTBT)	156, 48, 47
No. of BPM (ring, HEBT, RTBT)	44, 37, 17
No. of loss monitor (ring, HEBT, RTBT)	82, 62, 43
No. of current monitor (ring, HEBT, RTBT)	2, 5, 5
No. of profile monitor (ring, HEBT, RTBT)	4, 13, 8
Vacuum pressure, ring	10^{-8} Torr

ACCELERATOR DESIGN CHOICES

Accumulator ring

During the first year of construction, a study was performed comparing the present structure of full-energy linac plus accumulator ring to a rapid-cycling-synchrotron (RCS) design: a 60 Hz, 400 MeV linac feeds two, vertically stacked RCSs accelerating the proton beam to 2 GeV energy. The biggest challenge to the RCS design is from the stringent (1 W/m) beam-loss criterion: although relaxed by

* SNS is managed by UT-Battelle, LLC, under contract DE-AC05-00OR22725 for the U.S. Department of Energy. SNS is a partnership of six national laboratories: Argonne, Brookhaven, Jefferson, Lawrence Berkeley, Los Alamos, and Oak Ridge.

† jwei@bnl.gov

a factor of 5, still only 0.4% uncontrolled loss is allowed for a 2 MW beam power assuming 90% collimation efficiency. On the other hand, among existing rings the lowest loss of about 0.3% is achieved at LANL's PSR, a 800 MeV accumulator, as opposed to typical losses of a few to tens of percent in RCSs (e.g. ISIS, FNAL and AGS Boosters).

As opposed to the accumulator, the RCSs operating at 30 Hz require a high RF voltage (about 400 kV per ring at 1.4 - 1.9 MHz) for fast acceleration, a large magnet aperture to accommodate the space charge at a lower energy, ceramic vacuum pipes with detailed RF shielding, and high-performance power supplies. Minimization of magnetic errors due to eddy current, ramping, saturation, and power-supply tracking is non-trivial. The study concluded that the required RCS design is technically more demanding and less cost effective [4].

Permanent magnets were considered as an option for the accumulator ring magnets. Electromagnetic magnets were chosen instead, given the uncertainty in the linac energy. This choice is especially appropriate to accommodate later-adopted superconducting-RF linac.

Ring FODO-doublet lattice

The four-fold symmetric ring lattice contains four dispersion-free straights, each housing injection, collimation, RF, and extraction (Fig. 1). Each achromatic arc consists of 4 FODO cells with 90° horizontal phase advance.

After optimization, the ring lattice has doublet straights [1]. The lattice combines the FODO structure's simplicity and ease of correction with the doublet structure's flexibility for injection and collimation. Injection at a dispersion-free region allows independently adjustable painting in the transverse (with orbit bumps in the ring) and longitudinal (with an energy-spreading phase-modulated RF cavity in the HEBT) directions for a robust operation. The 12.5 m-long uninterrupted straight section with a flexible phase advance further improves collimation efficiency. Comparing with the original all-FODO lattice, matching between the arcs and the straights increases the arc acceptance by 50% with the same magnet aperture (Fig. 2).

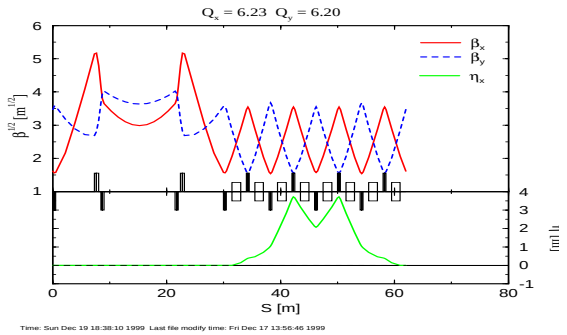

Figure 2: SNS ring FODO/doublet lattice.

Lessons learned

Solid-steel, as opposed to laminated-steel, was selected for most ring and transport magnet cores for cost savings.

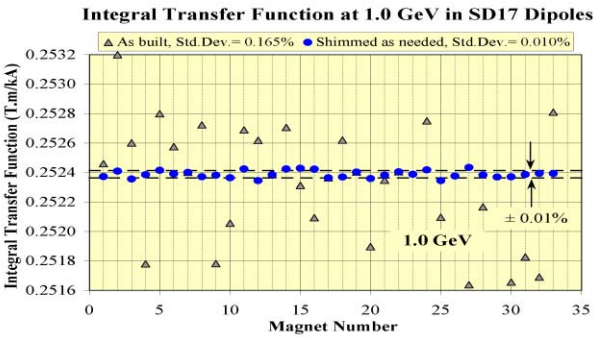

Figure 3: ITF Variation of the dipole magnets before and after shimming (courtesy P. Wanderer and A. Jain).

Individually, good field quality ($\sim 10^{-4}$ relative error at full acceptance) is achieved. However, excessive (up to 0.25%) magnet-to-magnet variation is found in the dipole integral transfer function (ITF) and its current dependence (Fig. 3) [5]. These dipoles are shimmed with iron sheets to achieve below 10^{-4} variation for 1 GeV operation, and sorted according to 1.3 GeV measurement data to minimize orbit corrector strength. Ring quadrupoles are partly sorted according to the power-supply family, and partly shimmed to achieve below 10^{-4} variation among each family.

The design does not allow in-situ baking of vacuum chambers that is needed for alternative NEG film coating.

PHYSICAL CHALLENGES

Main ring challenges include meeting the target requirements on the peak current density, minimizing uncontrolled beam loss, and controlling collective effects (space charge, instabilities, electron cloud [1].

Beam loss

Tables 2 and 3 list the expected controlled and uncontrolled beam loss. Beam collimation is performed at multiple locations (Fig. 1) to minimize the uncontrolled loss.

Space charge

The dominant collective effects are expected to be beam halo and beam loss generated by space-charge related res-

Table 2: Estimated controlled loss for a 2 MW beam.

Mechanism	Location	Fraction
HEBT:		
H^0 from linac	linac dump	10^{-5}
linac transverse tail	H/V-collimator	10^{-3}
linac energy jitter/spread	L-collimator	10^{-3}
Ring:		
beam-in-gap	BIG kicker	10^{-4}
excited H^0 at foil	collimator	1.3×10^{-5}
partial ionization at foil	injection dump	10^{-2}
foil miss	injection dump	10^{-2}
ring beam halo	collimator	1.9×10^{-3}
energy straggling at foil	collimator	3×10^{-6}
RTBT:		
kicker misfiring	collimator	10^{-5}

Table 3: Estimated uncontrolled loss of a 2 MW beam.

Mechanism	Location	Fraction	Power [W/m]
HEBT:			
H^- magnetic strip.	all HEBT	1.7×10^{-6}	0.02
collimator out-scatt.	achromat	7.5×10^{-6}	0.1
Ring:			
H^- magnetic strip.	inj. dipole	1.3×10^{-7}	0.3
nucl. scatt. at foil	foil	3.7×10^{-5}	2.5
collimation ineff.	all ring	10^{-4}	0.9
RTBT:			
nucl. scatt. at window	target window	4×10^{-2}	

onance crossing [6]. Other intensity-limiting mechanisms include electron-cloud effects and instabilities due to the extraction-kicker coupling impedance (Table 4).

The maximum incoherent space-charge tune spread is chosen to be 0.15 to avoid resonance-induced beam loss (Fig. 4). Transversely, the beam is painted to a full, unnormalized total emittance of 240 $\pi\mu$m. Longitudinally, a dual-harmonic RF system is used to achieve a bunching factor ~ 0.45, and HEBT energy spreader is used to paint a full momentum spread of $\pm0.7\%$ without enhancing tails.

Impedance and instabilities

Efforts are made to reduce the coupling impedance in a frequency range from about 200 Hz to above 50 MHz. 14 extraction kickers residing inside the vacuum chamber are major sources of transverse impedance. The impedance associated with the high-μ ferrite was reduced by terminating the pulse-forming network (PFN) circuit to 25 Ω, and by maximizing the width of the kicker module (Fig. 5).

Electron-cloud effects

Electron cloud remains to be an unresolved issue. Computer simulation indicates a trailing-edge electron concentration of peak value near 15 nC/m, much higher than the value simulated for the PSR ring [8].

Mitigation measures involve suppressing electron generation and enhancing Landau damping [9]. Magnetron (dc) sputtering is used to coat the surfaces with 0.1 μm TiN to reduce electron multipacting (Fig. 6). Electrons

Table 4: Collective effects and estimated thresholds for a 2 MW beam.

Mechanism	Threshold
Trans. space charge	$\Delta\nu_{sc} \approx -0.2$
Long. space charge	15 kV induced RF voltage
Trans. microwave instab.	$Z_\perp \approx 60$ kΩ/m
Long. microwave instab.	$\lvert Z_\parallel/n\rvert \approx 100\ \Omega$
Resistive wall	
($\xi = 0$)	$Z_\perp \approx 1.3$ kΩ/m at 200 kHz
($\xi = -3$)	$Z_\perp \approx 100$ kΩ/m at 200 kHz
Electron-cloud	above 2 nC/m

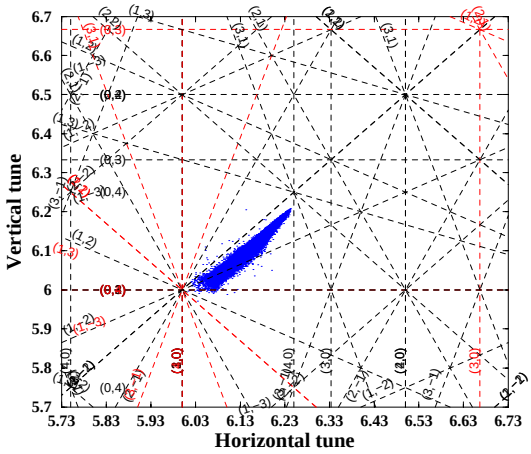

Figure 4: Transverse tune spread at the end of injection. Computer simulation is performed with UAL/ORBIT package [7]. Effects of space charge, transverse painting, chromaticity, kinematic non-linearity, fringe field, and magnetic manufacturing impections are included.

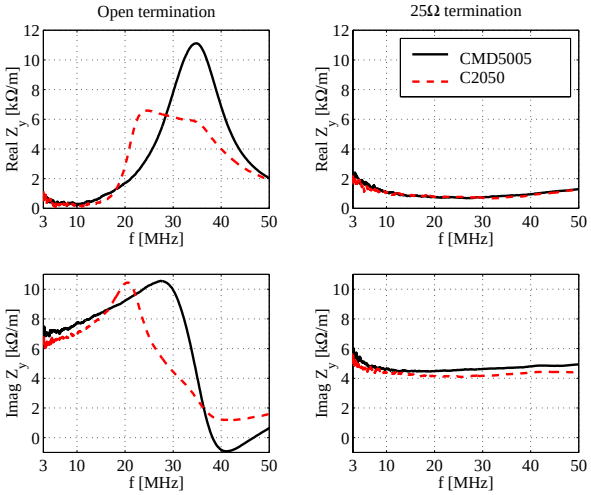

Figure 5: Comparison of measured coupling impedance for open and 25 Ω PFN termination, and high (1600) and medium (100) permeability ferrite of the extraction kicker (courtesy D. Davino and H. Hahn).

in the injection region are guided to the collectors with a low backscattering yield. A beam-in-gap kicker ensures a clean beam-gap. Vacuum ports are screened, and steps in the vacuum pipe are tapered to reduce peaked electric fields causing electron emission. A good vacuum reduces electrons from gas ionization. Solenoids are wound in the collimation sections to reduce multipacting. Electrodes are installed in the injection region (10 kV) and around the ring at BPM's (±1 kV) to clear the electron cloud. Electron detectors are installed at susceptible locations.

Enhancement of Landau damping includes a large vacuum chamber at locations of high dispersion and a large RF voltage to provide sufficient momentum acceptance, longitudinal painting to expand the momentum spread of the injecting beam, and lattice sextupole families for chromatic adjustments. Finally, a fast, wideband feedback system is

planned to damp instabilities.

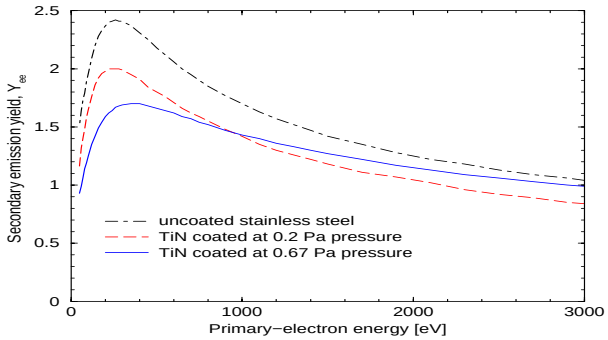

Figure 6: Measured secondary-electron yield for various coating conditions (courtesy P. He, H. Hseuh et al).

TECHNICAL ISSUES & STATUS

Injection

For charge-exchange injection of an intense H^- beam, free-hanging carbon and diamond foils are both developed to be mounted on a quick-exchange mechanism [10]. Stripped electrons are guided by the fringe field of tapered magnets and collected by heat-resistant C-C material attached to a water-cooled copper plate (Fig. 7). Both stripping foils and the electron catcher are monitored by video systems.

The transverse painting is achieved by 4 horizontal and 4 vertical dipoles with programmable power supplies. The measured minimum rise time (about 175 μs) is below the design value. The longitudinal painting is achieved by using a RF cavity located in the HEBT that is phase modulated with respect to the linac frequency.

Collimation

The H^- beam in the HEBT is cleaned with stripping foils, and then a magnetic field separates the stripped beam from the original H^- beam. The transverse collimation is located at the end of the linac upstream of the energy corrector, and the longitudinal collimation is located in the 90° bend achromat.

The proton beam in the ring is cleaned transversely with a two-stage system, wherein the primary scraper scatters the beam and enhances its impact distance in the secondary collector, so achieving a cleaning efficiency above 90%. The primary scraper consists of four tantalum blades, each 5 mm thick. They are spaced in 45 degree angles, adjustable to the varying needs of collimation aperture, and shielded for containing radioactivity. Due to reliability considerations, the secondary collectors are non-adjustable. Their vacuum chambers are made of double-layered stainless-steel filled with helium gas between the layers to detect leaks [11]. Longitudinally, the proton halo moved into the beam gap is cleaned by the beam-in-gap kicker and collected by the two-stage collimation system during the last 100 turns before extraction.

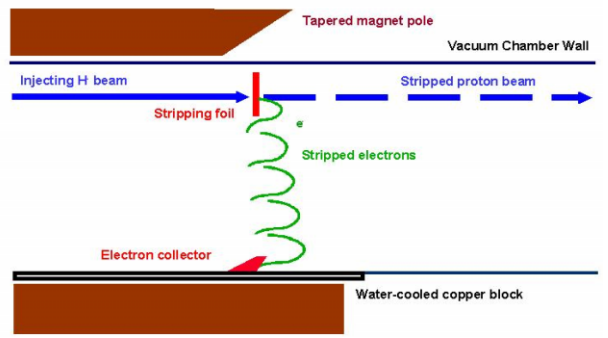

Figure 7: Injection area schematic layout.

Extraction

The beam is extracted during a single turn by being kicked vertically into the extraction channel of septum magnet. The septum bends the beam horizontally, and is also rotated to correct the vertical kicks. The kicker system consists of 14 individually powered modules, so that beam loss is negligible when one module fails. The PFNs are installed outside the ring tunnel for easy maintenance. The phase advance between the extraction kicker and the target is chosen so that the beam's position on target does not change if errors develop with the kickers.

To avoid complications due to rapid variations of the magnetic field, kicker magnets are made with a single-turn coil-winding and are placed inside the vacuum chamber. Good field quality is achieved with a high-permeability ferrite material. Saturable inductors isolate the influence of the PFN, shorten the rise time, and improve the flatness of the kicker-pulse's waveform. Beam density dependent closed-orbit deviation induced by the extraction kicker coupling-impedance at the given beam offset ("banana-closed orbit") is about 1 mm.

Vacuum and chamber coating

The design vacuum pressure is $(0.5 \sim 1)\times10^{-7}$ Torr in HEBT to minimize H^- stripping, 10^{-8} in the ring to minimize gas scattering and ion- and electron-induced desorptions, and $(0.5 \sim 1)\times10^{-7}$ Torr in RTBT.

The entire inner surface of ring vacuum chamber and extraction kicker ferrite is coated with TiN [9]. Two layers of coating are applied to the ceramic chamber for injection kickers: a 1μm-thick copper layer for by-passing the image charge, and a 0.1μm-thick TiN layer for a low secondary-electron yield, along with an exterior metal enclosure for dc current by-pass. This design allows the image-current passage above the lowest betatron sideband (∼200 kHz) without degrading the magnetic-field penetration, eddy-current heating, and beam-induced heating.

Magnet, correction, power supply

Iterations are made on almost all kinds of magnets towards design expectation of magnetic accuracy at 10^{-4} for main dipoles and quadrupoles, 10^{-3} for sextupoles, chicane and transport magnets, and 10^{-2} for correctors. Some exceptions include a large (0.19×10^{-2}) systematic 20th

Table 5: Measured integral multipoles of the ring dipole magnet at a reference radius of 80 mm. The systematic b_1 is due to tapered dipole ends.

n	b_n		a_n	
	mean	S.D.	mean	S.D.
0	10000	0.0	0.0	0.0
1	-105.041	0.275	-0.262	0.951
2	0.163	0.433	-0.020	0.494
3	2.051	0.149	-0.050	0.316
4	1.143	0.200	0.000	0.113
5	0.064	0.095	0.001	0.158
6	-0.300	0.120	-0.017	0.105
8	-0.077	0.107	0.005	0.056
10	-0.176	0.129	0.003	0.028
12	0.094	0.143	-0.006	0.047

Table 6: Measured multipoles of the ring quadrupole magnet at a reference radius of 80 mm.

n	b_n		a_n	
	mean	S.D.	mean	S.D.
1	10000	0.00	–	–
2	-0.30	1.11	0.41	1.20
3	-0.06	0.58	0.05	0.32
4	-0.01	0.20	-0.04	0.23
5	1.20	0.25	-0.11	0.15
9	-0.73	0.02	0.00	0.06
13	-0.06	0.01	-0.01	0.02

pole on narrow-width quadrupoles used in the straights whose effects are negligible during the 1 ms accumulation, and large (6%) decapole in multi-coil skew-sextupole correctors [12].

Four-family sextupoles are arranged in 4-fold ring lattice symmetry for chromaticity adjustment without compromising the dynamic aperture. The ring correction elements consist of horizontal and vertical dipoles, normal and skew quadrupoles, normal and skew sextupoles, and octupoles for orbit correction and decoupling, amplitude detuning, and resonance corrections. Octupoles can be rotated to act as skew-octupoles if needed. The reduction in quadrupole transfer function ($\sim -0.2\%$) caused by the interference from nearby sextupole/corrector is easily adjusted. Resonance correction strategy is developed in the presence of space charge [6].

There is 1 power supply for the main dipoles, 6 for the quadrupoles, 4 for the sextupoles, 115 for the correctors and chicane dipoles, 8 for the injection kickers, and 14 for the extraction kickers. Good rise/fall time and matching have been achieved on pulsed supplies (programmable injection and extraction) [13].

RF system

The HEBT has two RF cavities operating around linac frequency of 805 MHz, one for energy correction and the other for longitudinal painting. The ring dual-harmonic RF system maintains a gap for the rise time of the extraction kicker while maintaining low peak beam current and large momentum spread, reducing space charge stopband related losses and coherent instabilities [14].

Diagnostics

The ring and transport diagnostics consists of beam position monitor, loss monitor, current monitor, wire scanner, beam-in-gap monitor, foil/catcher video monitor, ionization profile monitor (IPM, Fig. 8), coherent/incoherent tune measurement system, and electron detector [15].

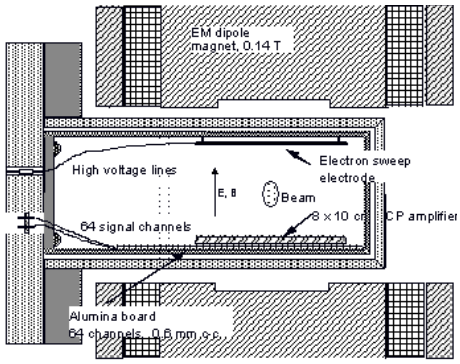

Figure 8: Ring IPM with sweeping electrodes, and with the multi-channel plates for electron collection recessed from the vacuum-chamber wall to avoid superfluous signals (courtesy R. Connolly).

Reliability and availability

Engineering design considers redundancy, radiation resistance, "active maintenance" capability (all-around cranes, quick-release flanges, quick-release water fittings, moveable shielding), and spares for areas of high radiation and activation.

FUTURE PERSPECTIVES

The ring and transport facility is designed with the potential to reach a beam energy up to 1.3 GeV and a beam power beyond 2 MW, capable of supplying a second neutron target [1]. Space is reserved for two additional extraction kickers, and for the replacement of 2 injection-chicane dipoles to satisfy H^0 stripping conditions.

We are indebted to the SNS teams and our collaborators for their devotion and contributions.

REFERENCES

[1] J. Wei et al, PRST-AB, **3** (1999) 080101; J. Wei, Rev. Mod. Phys. (Oct. 2003)
[2] N. Holtkamp, these proceedings
[3] N. Catalan-Lasheras et al PRST-AB **4** (2001) 010101
[4] J. Wei et al, EPAC00 (2000) 981
[5] P. Wanderer et al, these proceedings
[6] A. Fedotov, these proceedings
[7] N. Malitsky, these proceedings; J. Holmes, these proceedings
[8] M. Pivi, M. Furman, PRST-AB, **6** (2003) 034201
[9] M. Blaskiewicz; S.Y. Zhang et al; J. Wei et al, these proceedings; P. He et al, submitted to J. Vac. Sci. Tech. (2003)
[10] R. Shaw et al, these proceedings
[11] H. Ludewig et al; N. Simos et al, these proceedings
[12] J. Tuozzolo et al; N. Tsoupas et al; S. Badea et al; C. Pai, et al; J. Rank, et al, these proceedings
[13] J. Sandberg et al; W. Zhang et al, these proceedings
[14] A. Zaltsman et al; K. Smith et al, these proceedings.
[15] P. Cameron et al; M. Kesselman et al; D. Gassner et al; R. Connolly et al; R. Witkover et al, these proceedings.